Composite Structures 290 (2022) 115513

Contents lists available at ScienceDirect

Composite Structures

journal homepage: www.elsevier.com/locate/compstruct

Synchronous deployed design concept triggered by carbon fibre reinforced shape memory polymer composites

Dou Zhang [a], Liwu Liu [a], Xin Lan [b], Jinsong Leng [b,*], Yanju Liu [a,*]

[a] Department of Astronautical Science and Mechanics, Harbin Institute of Technology, Harbin 150001, People's Republic of China
[b] Centre for Composite Materials and Structures, Harbin Institute of Technology, Harbin 150080, People's Republic of China

ARTICLE INFO

Keywords:
Shape memory polymers
Carbon fibre reinforced polymers
Three-point bending
Synchronous deployments
Symmetrical structures

ABSTRACT

Synchronous deployments for symmetrical structures such as solar arrays and antennas are desired because they are conducive to subsequent attitude stabilization. In this work, we propose a synchronous deployed mechanism triggered by shape memory polymer composites (SMPCs). Firstly, the material design was developed according to the fibre microbuckling behaviour of unidirectional carbon fibre reinforced laminates undergoing flexural deformation to balance high mechanical requirements and large deploy/fold ratio desirements. Then, two resins with different glass transition temperatures (*Tgs*) from a similar shape memory epoxy system were used for fabrication. These laminates with different fibre volume fractions, thicknesses, matrices and fibre distributions were tested by three-point bending tests to evaluate their mechanical performance. Recovery tests were carried out under different environmental temperatures. In addition, the recovery stimulated by resistor heaters in vacuum endowed the mechanism with good recovery robustness. Finally, functional validation on an aluminium prototype showed good synchronization. This design concept has the advantage of being lightweight, low-impact and highly reliable. It is expected to provide a reasonable and robust solution for synchronous deployments.

1. Introduction

Deployable subsystems are required in nearly every modern spacecraft, whether in the form of a solar array [1], an antenna [2,3], a radiator [4,5], a solar sail [6] or a sunshade. The history of deployable structures can be traced back to the 1960s. The echo balloon series and flexible solar array (FRUSA) were significant milestones in deployable aerostructures [7]. Thereafter, the inflatable technology was also an important step forward [8]. It is anticipated that with an increasing diversity of functionality, spacecrafts with novel deployable architectures are desired. Shape memory polymers (SMPs) and their composites (SMPCs) have received considerable attention from the research community in recent years. SMPs are a typical kind of smart materials which can maintain a designed temporary configuration and recover their original shape spontaneously under specific external stimuli, such as heat, light, electricity, magnetism, water and change of pH [9]. This self-recovery property makes them ideal for deployable structures. Although compared with shape memory alloys (SMAs), they have greater deformation bearing capacity and lower manufacture costs, the deficiency of insufficient load capacity limits their applications in aerospace[10]. By adding enhancements such as particles and fibres into the polymer matrix, composites are prepared. Carbon fibres are widely used to reinforce polymers due to their high strength, lightweight, good thermal and electrical conductivities [11]. Carbon fibre reinforced polymers (CFRPs) possess excellent mechanical properties and have been widely used [12]. Carbon fibre reinforced SMPCs have been applied to self-deployable mechanisms in different structural forms, such as hinges, antennas, hold and release mechanisms (HRMs) and solar panels [13].

Deployable architectures with reduced mass, increased packaging efficiency and deployable reliability are desired to fulfil new mission demands. Existing deployments are actuated usually by strain energy stored in elastic spars or spring hinges. An appropriate HRM that directly affects deployable modules' function is a vital facet of these subsystems. Hence, a significant effort is dedicated to its design. Traditional HRMs are generally triggered by pyrotechnics, possessing instantaneous operation and little input energy. A typical example of them is explosive bolts [14], which are experienced and flight-proven. However, the impact caused by the explosion cannot be ignored, and thus satellites are required with high-level impact bearing capacity. This inevitable impact will introduce additional challenges for satellite design and attitude stabilization, especially for small and nano satellites. Another solution, the paraffin actuator, providing large strokes and high actuation force, is

---

* Corresponding authors.
E-mail addresses: lengjs@hit.edu.cn (J. Leng), yj_liu@hit.edu.cn (Y. Liu).

https://doi.org/10.1016/j.compstruct.2022.115513
Received 29 September 2021; Received in revised form 3 March 2022; Accepted 21 March 2022
Available online 23 March 2022

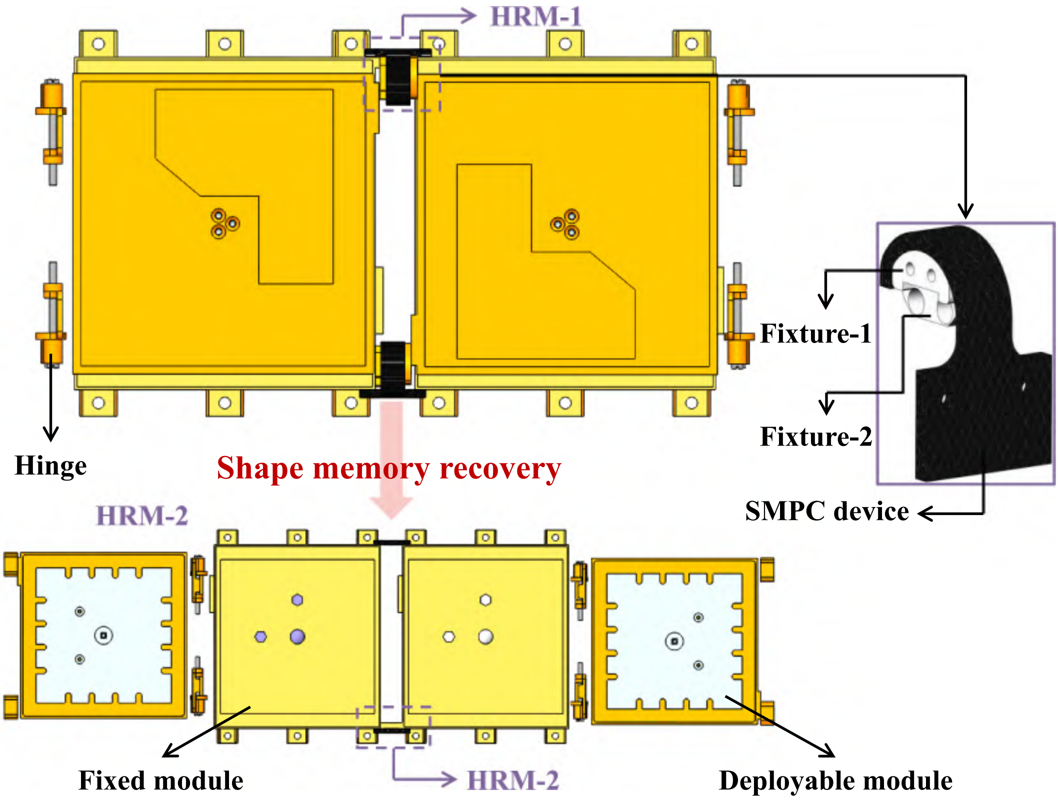

Fig. 1. Schematic of synchronously deployable structures.

achieved by the incompressible volume expansion associated with the solid–liquid phase transition [15]. This simple actuation principle predestinates a slow operation and voluminous architecture. The Kevlar cord and thermal knife element is also a practical plan [16]. While the major issues, such as Kevlar cord pre-tension and relaxation, and thermal knife failure, must be carefully considered in the design practice.

These non-explosive structures all consume a significant amount of actuation time and a considerable amount of energy. Besides, these disposable constructs can neither be tested again nor reused or recycled, resulting in low repeated reliability and high cost. Thus, HRMs with rapid actuation, low impact and repeatable usage are proposed. A non-explosive release actuator relying on an SMA wire and segmented nuts allows high preload (15kN) and low levels of shock (350G) for deployable solar arrays [17]. This device can be easily and instantly reset after actuation, thanks to the shape memory effect of the SMA wire. Neither refurbishment nor replacement of any components is needed. This reusable mechanism can also be made from SMPCs and be lighter in weight. By employing temporally deformed inner and outer SMPC cylinders, HRMs with multiple configurations have been presented to separate two components [18,19]. The latching force is tested by tension tests, and structural parameters can be readjusted according to mission requirements. An ultra-light HRM holding the deployable solar panel through bending deformation is designed and tested [20]. Compared with SMAs, these HRMs composed of SMPCs can withstand tremendous strains, facilitating the design. Besides, these structures are intrinsically lighter. Although in our previous work [20], solar arrays are successfully deployed, the two symmetrical panels on the CubeSat cannot be released strictly at the same time. This sequence can bring new challenges to the following attitude control of the satellite. Therefore, despite the high challenge of developing synchronous deployed mechanisms, the payoff and potential applications should not be overlooked. A solar sail subsystem can be deployed simultaneously by a simple method where both the masts and membrane films are unfolded in a deterministic way to demonstrate a high robust mechanism [21,22]. Such synchronous deployment is designed for integrated structures. However, new schemes to fulfil the synchronization for symmetrical systems are urged.

The design concept in this work aims to improve the HRM proposed in our previous work [20] in terms of deployable synchronization. Firstly, a structure with two symmetrical deployable modules is designed. It can either be a small satellite or a subsystem such as an antenna or a solar array. Then, materials are designed according to the microbuckling behaviour of carbon fibres when composites are undergoing flexural deformation. Besides, two resins with different glass transition temperatures (*Tg*s) from the same shape memory epoxy system are used to prepare composites. Thereafter, three-point bending tests are conducted to characterize the material bending properties. Finally, shape memory recovery tests and release demonstration show preliminary functional validation.

2. Design and fabrication

2.1. Structure design

A symmetrical deployed structure that consists of two identical deployable modules is shown in Fig. 1. Each module is connected to two HRMs. The HRM is comprised of an SMPC device and two fixtures (fixture-1 and fixture-2), which complement each other geometrically and are attached to the left and right deployable modules, respectively. The SMPC device is connected to the fixed module through a screw. The temporarily curved SMPC devices package deployable modules during the transportation and storage stage. When the satellite is in orbit, SMPC devices will be stimulated by external power and recover their original plate shape. Thus, the deployable modules will rotate under the effect of spring hinges and finish the deployment. The envelope size of the structure changes from 33 mm × 24.84 mm × 23.55mm to 58.22mm × 24.84mm × 4.66mm. For a large deploy/fold ratio, the bending radius of the SMPC release device is fixed to 10 mm as the mission required. This design can ensure the synchronization effectively

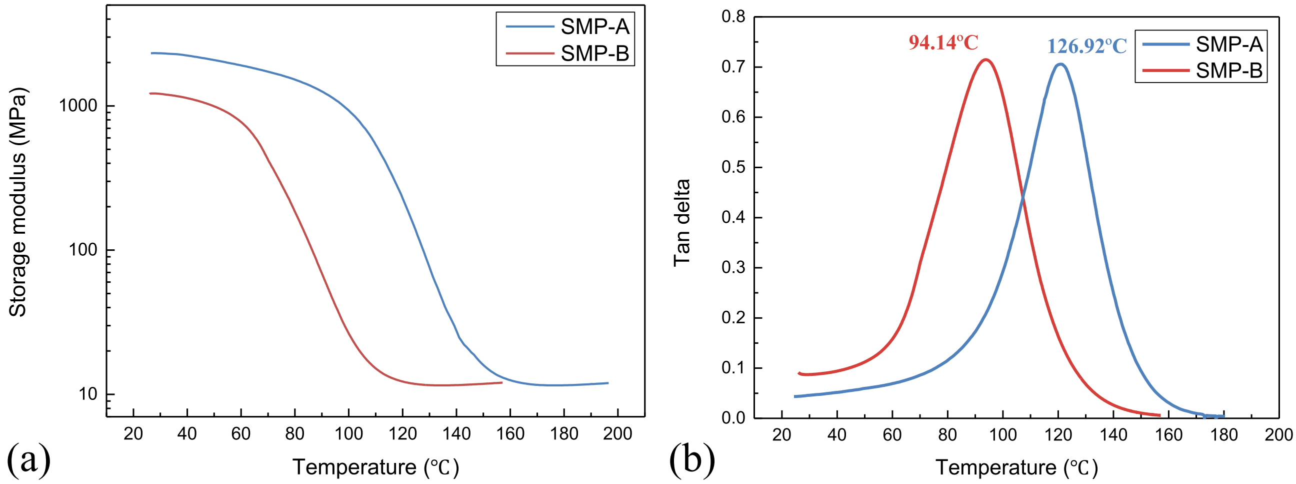

Fig. 2. Dynamic mechanical analysis of SMP-A and SMP-B, (a) storage modulus and (b) Tan delta versus temperature curves.

by using a symmetrical installation of two HRMs.

2.2. Material design

It is well known that both the higher space utilization (larger deploy/fold ratio) and better locking effect (higher flexural stiffness) are desired. However, these two requirements are contradictory for the material design. Lower fibre volume fraction and thinner laminate are preferred for a larger deploy/fold ratio to prevent material failure. While to achieve higher flexural stiffness, higher volume fraction and thicker laminate are recommended. The compromise between the large deploy/fold ratio and high flexural stiffness can be found with fibre microbuckling analysis. Firstly, fibres are assumed to microbuckle in-plane in a sinusoidal shape, and the shape function is written as:

$$y = A\cos\frac{\pi x}{\lambda} \tag{1}$$

The half-wavelength λ and amplitude A are two undetermined parameters. Lan et al. [23] first zoned the cross-section into three areas: non-buckling stretching, non-buckling compression, and buckling compression zones. The total strain energy is made up of four parts: fibre buckling strain energy U_f, shearing strain energy U_{xy} of the matrix, shearing strain energy U_{yz} of the matrix, and stretching and compression strain energy U_{xx} of the laminate. Then, the self-consistent approach is adopted according to the minimum energy principle to obtain a series of expressions of key parameters. The half-wavelength of the buckled fibres is expressed as:

$$\lambda = \begin{cases} +\infty, \ \kappa < \kappa_c \\ \left[\dfrac{8\pi^3 v_f E_f I_f \left({z_{ns}}^2 - \frac{4M^2}{\kappa^2}\right)}{v_m G_m {d_f}^2 \ln\left(\frac{\kappa z_{ns}}{2M}\right)}\right]^{1/4}, \quad \kappa \geq \kappa_c \end{cases} \tag{2}$$

$$M = \frac{v_m G_m}{v_m E_m + v_f E_f} \tag{3}$$

$$\kappa_c = \frac{4}{t} M \tag{4}$$

where v_f and v_m denote the fibre and matrix volume fractions, and they satisfy the relationship of $v_f + v_m = 1$. E_f and E_m represent Young's moduli of the fibre and matrix, respectively. I_f is the cross-section moment of inertia, and for circular fibres, it can be written as:

$$I_f = \frac{\pi {d_f}^4}{64} \tag{5}$$

where d_f is the diameter of circular fibres. z_{ns} signifies the location of the neutral surface and can be expressed as:

$$z_{ns} = \begin{cases} \dfrac{t}{2}, \ \kappa < \kappa_c \\ t - \dfrac{M}{\kappa}\left(\sqrt{1 + \dfrac{2\kappa t}{M}} - 1, \quad \kappa \geq \kappa_c\right. \end{cases} \tag{6}$$

κ labels the curvature of laminates. κ_c is the critical buckling curvature, which means at this point, fibre initiates microbuckling, and t is the thickness of laminates. The material parameter M is determined by components of composites. Besides, the temperature, which significantly influences the shape memory matrix's modulus, also affects this parameter. This temperature-dependent characteristic will be illustrated later by the polymer's dynamic mechanical analysis and isothermal tension tests. The shear modulus of the matrix G_m meets the following relationship:

$$G_m = \frac{E_m}{2(1 + \upsilon_m)} \tag{7}$$

where υ_m represents the Poisson's ratio of the polymer matrix. The amplitude of buckled fibres in the compressive buckling zone can be deduced as:

$$A = \begin{cases} 0, \ \kappa < \kappa_c \\ \dfrac{2\sqrt{\kappa(z_{ns} - z)}}{\pi}\left[\dfrac{8\pi^3 v_f E_f I_f \left({z_{ns}}^2 - \frac{4M^2}{\kappa^2}\right)}{v_m G_m {d_f}^2 \ln\left(\frac{\kappa z_{ns}}{2M}\right)}\right]^{1/4}, \quad \kappa \geq \kappa_c \end{cases} \tag{8}$$

The maximum radius of curvature at the vertex of sinusoidal fibres is:

$$R_f = \frac{\lambda^2}{\pi^2 A} \tag{9}$$

Fibres are assumed to undergo only pure bending, and therefore the maximum strain of buckled fibres $\varepsilon_{f,max}$ can be deduced as:

$$\varepsilon_{f,max} = \frac{1}{R_f}\frac{d_f}{2} \tag{10}$$

On the inner surface of laminates where $z = 0$, fibres show the most considerable amplitude, which is also where fibres are most vulnerable to fracture. The strain of fibres here is:

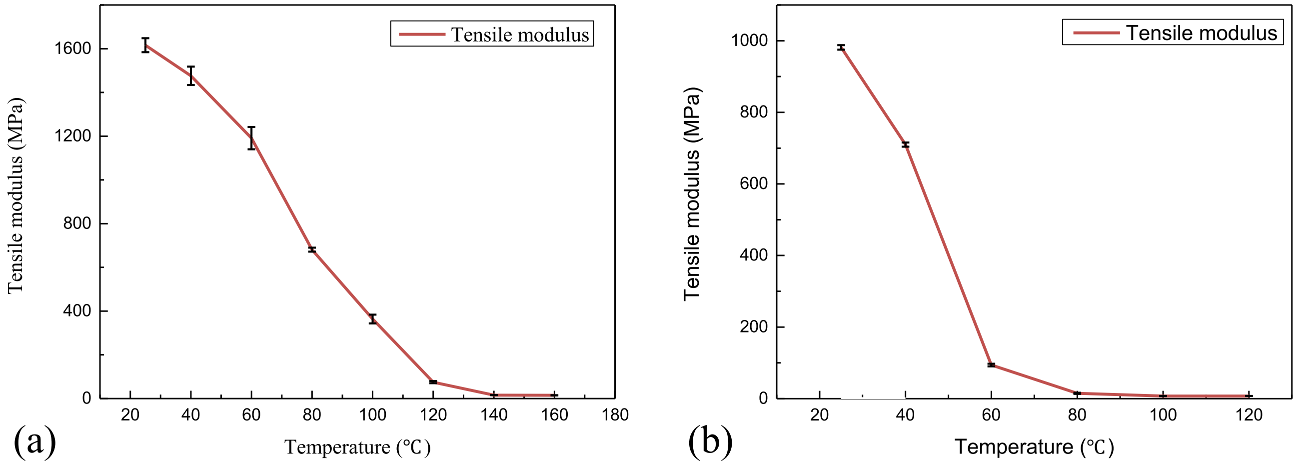

Fig. 3. Tensile modulus versus temperature curves of (a) SMP-A and (b) SMP-B.

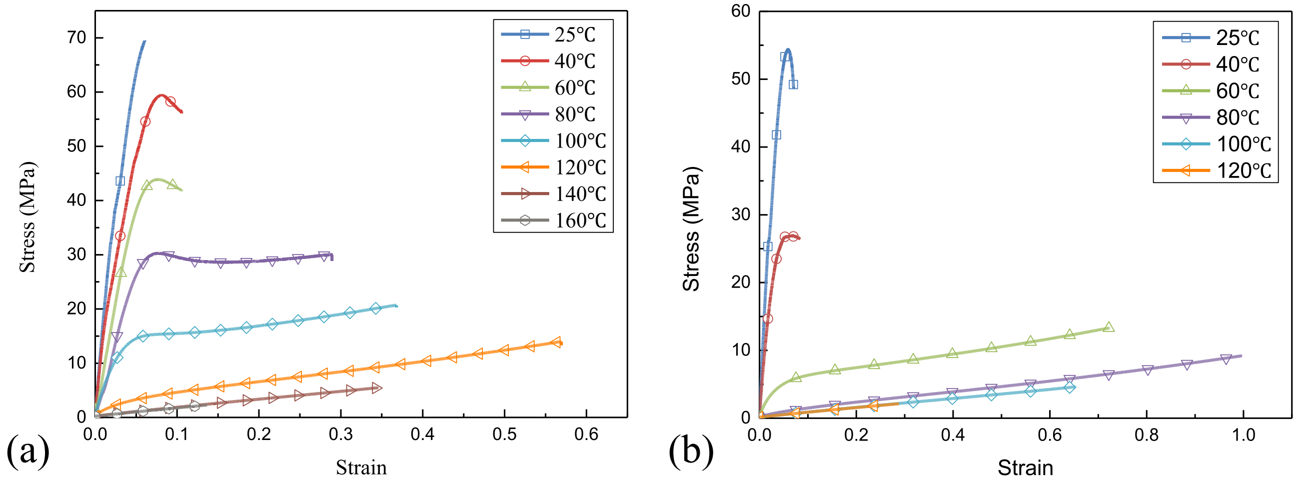

Fig. 4. Tensile stress versus strain curves of (a) SMP-A and (b) SMP-B.

$$\varepsilon_{f,max}(z=0) = \kappa\left[\frac{8G_m v_m {d_f}^2 N^2 \ln\left(\frac{\kappa N}{2M}\right)}{E_f v_f\left(-4M^2+\kappa^2 N^2\right)}\right]^{\frac{1}{4}} \tag{11}$$

$$N = t - \frac{M\left(-1+\sqrt{1+\frac{2\kappa t}{M}}\right)}{\kappa} \tag{12}$$

The fibre will break when:

$$\varepsilon_{f,max}(z=0) = \varepsilon_{f,failure} \tag{13}$$

Synthesizing the above analysis, the modulus ratio of fibre and matrix E_f/E_m, fibre volume fraction v_f and laminate thickness t are three key parameters for material design. Hence, in this work, we choose two epoxy-based shape memory matrices from a similar resin system, SMP-A and SMP-B, which have different Tgs and moduli at the same temperature. These two polymers were tested both by dynamic mechanical analysis and static tension tests. Firstly, dynamic mechanical analysis was conducted on a DMA analyser (NETZSCH Instruments, Germany) with a tension mode at a heating rate of 3 °C/min and a frequency of 1 Hz. The storage modulus as a function of temperature is depicted in Fig. 2 (a). These two curves both show a relatively stable value at low temperature, representing the glassy state. With the temperature increasing, the storage moduli exhibit a rapid fall, which means the matrial undergoing the glass transition process. Finally, they go into the rubbery state where storage moduli show an about 100 times decline. This transition process can also be explained by the change of Tan delta in Fig. 2 (b). The Tan delta represents the loss factor which can be calculated by the ratio of the loss modulus to storage modulus. The temperature corresponding to the peak value of Tan delta is regarded as the Tg, and they are 126.92 °C for SMP-A and 94.14 °C for SMP-B.

Static isothermal tensile tests can also study this temperature-dependent stiffness property on a Zwick/Rolle 010 universal testing machine with a 1 kN load cell. Coupons were cut into dumbbell shape according to ASTM D638 type IV and heated by a thermal chamber. Samples were grouped into eight (SMP-A) and six (SMP-B) categories with intervals of 20 °C, except for room temperature, which was not 20 °C but about 25 °C. The strain rate was $0.67 \times 10^{-2} s^{-1}$, consistent with the literature [24]. Tensile modulus in Fig. 3 shows noticeable softening with temperature increasing, while it shows a negligible difference when higher than Tg. In Fig. 4, the strain at break first increases with temperature while it decreases when higher than Tg. This is because the mechanical properties of epoxy-based shape memory polymers are not only temperature-dependent, but also strain rate-dependent. We keep the same strain rate when conduct the tensile tests to obtain the temperature-dependent properties. At temperatures higher than Tg, when the strain rate is relatively high, there is not enough time for the soft molecular chain segments to stretch before the material breaks, resulting in a significant decrease in the elongation. More details about the rate-dependent properties can be seen in the literature [24], where the epoxy-based SMP is from the same system with the Tg of 92.17 °C.

Table 1
Physical properties of carbon fibre reinforcements.

Product No.	Filament	Fibre diameter (μm)	Tensile modulus (GPa)	Elongation (%)	Tensile strength (MPa)
T300B-1K	1000	7	230	1.5	3530
T300B-3K	3000				
T400HB-6K	6000	7	250	1.8	4410

When the strain rate is $0.33 \times 10^{-2} s^{-1}$, the strain at break increases with the temperature. While when the strain rate is $0.67 \times 10^{-2} s^{-1}$, the strain at break reaches a peak at 80 °C and then shows a decrease at 100 °C. In this paper, the strain at break maximizes at the temperatures 5–15 °C below *Tg*, i.e. 120 °C for SMP-A, and 80 °C for SMP-B. Therefore, these two temperatures are regarded as suitable to mould laminates to avoid material failure.

The effect of fibre volume fraction is another factor that influences the bending behaviour of laminates. It has been studied in the literature [23] that for laminates with a fibre volume fraction of 20%, fibre fracture is observed when the radius of bending curvature reaches the required 10 mm. Therefore, the fibre volume fraction is designed significantly lower than the previously studied one. Four values of 2.1%, 4.2%, 6.4%, and 12.8% are selected in fabrication, which will be illustrated detailly in the following subsection. Furthermore, the thicknesses of 2 mm and 3 mm are used to investigate their effect on bending performance.

Fibres used in this study are Toray's Torayca yarns T300B-1K, T300B-3K and T400HB-6K [25]. The physical properties of these reinforcements are listed in Table. 1. Therein, some differences are observed between T300B and T400HB, such as tensile modulus, strength and elongation. In fact, T300B-6K is desired to control variables, but it is not available. Therefore, T400HB-6K is used as a substitute. The different tensile moduli do affect the microbuckling behaviour of fibres. While fortunately, these differences are within 9% and can be used for a preliminary analysis.

2.3. *Material preparation*

A modified filament winding fabrication method [26] has been proposed by Li et al., which can obtain a uniform fibre distribution and controllable thickness. In this way, however, a filament winding machine is necessary to produce dry unidirectional carbon fibre layers. We modified this preparation technique to manually obtain uniformly distributed fibre layers, calling it the manual filament winding method. In the literature [26], the rotating mandrel consists of a rectangular plate that fibres wind on when the handle is rotating with a spindle. Two layers of fibres are produced at a time. When a winding is finished, the filler strips are stuck at edges, vertical to fibre orientation, continuing the next winding. Dry carbon fibre layers obtained by this method are evenly distributed. However, the fibres cannot be firmly fixed during curing due to the need to remove the fibre layers from the rectangular plate. The subsequent resin infusion process will also make fibres deviate from their original position. We refine the rotating plate into a hollow rectangle with marginal denticulations on the top and bottom to fix fibres throughout the winding and curing process. As shown in Fig. 5, these serrated edges were in two rows on each edge, which were the key to control uniform and straightened fibre layers without a machine. Similarly, each winding produced two layers. Filler strips were stuck at the edges between two winding units, which consisted of a rotating plate and two fibre layers. All winding units were then placed in the middle of the curing mould sealed with silicon strips. Finally, epoxy-based SMP resin was poured into the assembled mould from the upper opening. The curing process was conducted at 80 °C for 3 h, 100 °C for 3 h and 150 °C for 5 h. Laminates were then de-moulded and cut by a CNC engraving and milling machine into the desired shape. This manual filament winding is suitable for small-scale fabrication without a winding machine.

As one of the most common defects in fibre reinforced composites, the porosity weakens their mechanical properties. Therefore, the porosity of the laminates is examined by the microscope observation,

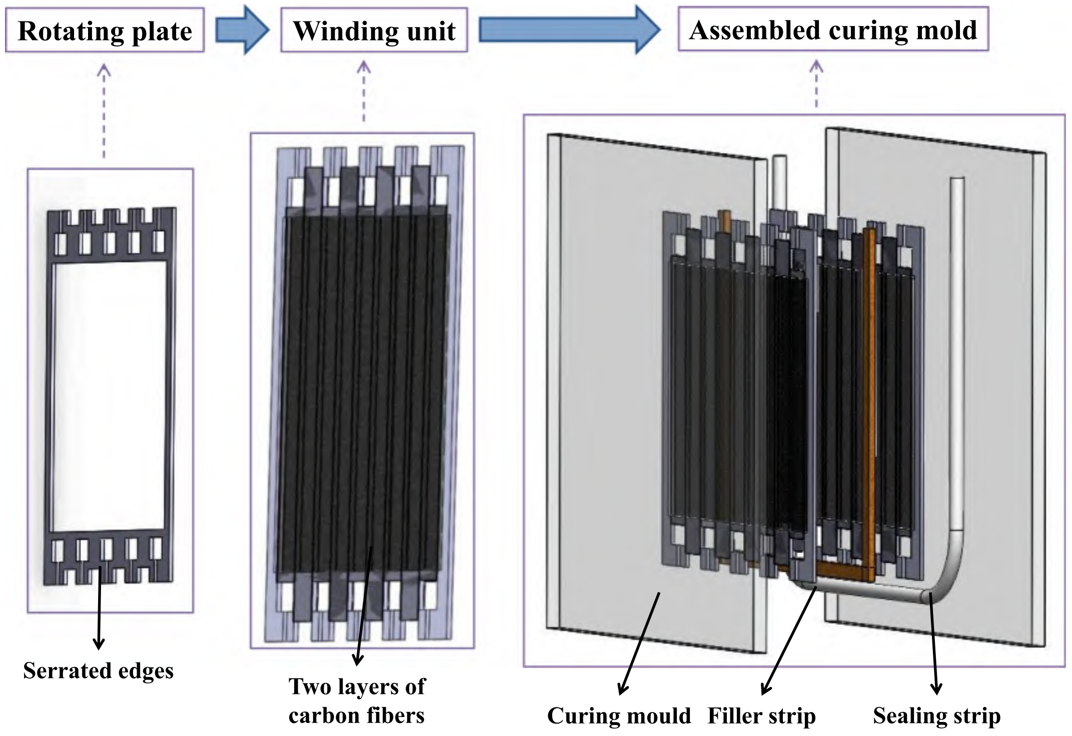

Fig. 5. Diagram of the manual filament winding preparation process.

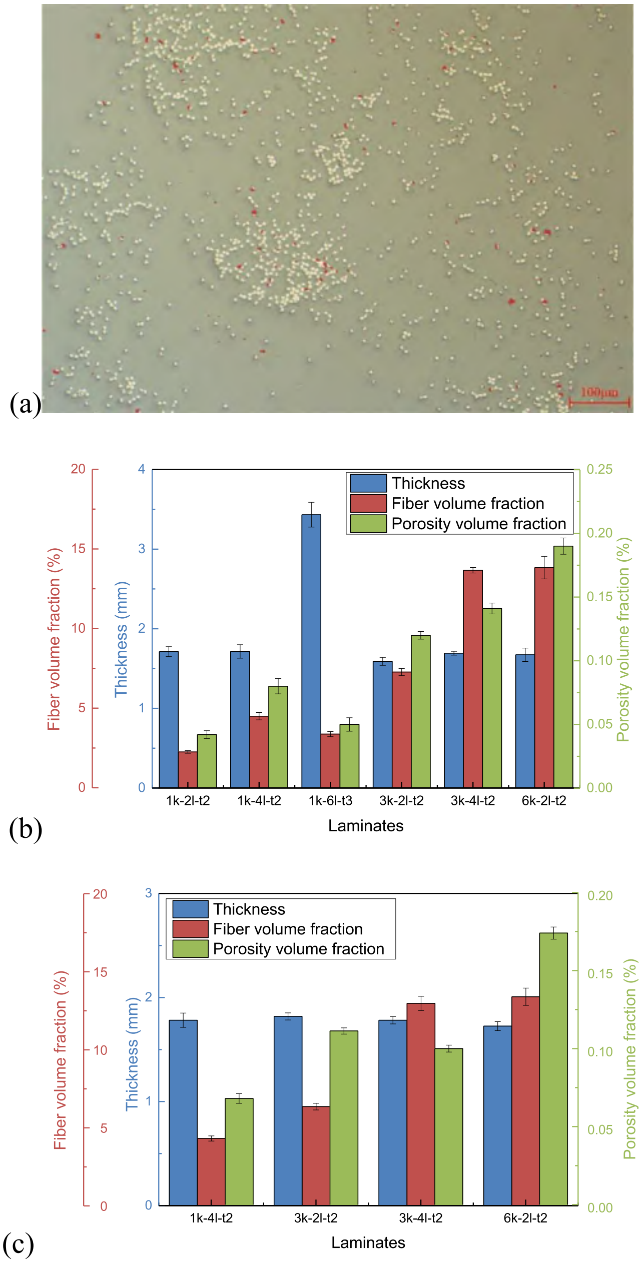

Fig. 6. (a) The microscopy image with porosity highlighted in red of 1k-4l-t2-SMP-B. Thickness, fibre volume fraction and porosity volume fraction for different laminates with the matrices of (b) SMP-A and (c) SMP-B.

which is a widely used technique [27]. At least three samples dimensioned in 10 mm in width, 10 mm in length and the whole thickness for each set of laminates were cut randomly from the panels and embedded in epoxy matrix holders. The cross-sections of these samples were then polished using grids of 600, 1200, 2500 and 4000, and the 6μm monocrystalline diamond suspension to obtain the smooth surface. An optical microscope (Nikon digital camera D5200) was used to observe and capture images. A microscopy image of 1k-4l-t2-SMP-B is demonstrated in Fig. 6 (a) with porosity highlighted in red for illustration. The voids disperse randomly between fibres. Ten types of carbon fibre reinforced SMPC laminates have been fabricated, of which the thickness, fibre volume fraction and porosity volume fraction have been shown in Fig. 6 (b) and (c). The fibre and porosity volume fractions are defined as the area ratios of the fibre and pore regions to the whole cross section, respectively. Three parameters label each laminate. The first is the fibre filament, the second represents the number of fibre layers, and the last denotes laminate thickness. The porosity volume fraction shows an upward trend with thicker fibre bundles due to the fibre clustering and relatively poor infiltration. Nevertheless, for all laminates studied in this work, the porosity volume fraction is less than 0.2%, smaller than a quarter of that in the literature [27]. This indicates that the materials prepared using the manual filament winding method are of good quality. Three filament types (1k, 3k, 6k), two thicknesses (2 mm and 3 mm) and four fibre volume fractions (2.1%, 4.2%, 6.4% and 12.8%) are considered. Along with two polymer matrices, the effect of four variables can be analysed in Table. 2. The effect of fibre property and fibre distribution is integrated for the reason mentioned previously.

Table 2
Sample groups to analyze four factors influencing material properties.

Influencing factors	Sample groups
Matrix	1k-4l-t2-SMP-A & 1k-4l-t2-SMP-B 3k-2l-t2-SMP-A & 3k-2l-t2-SMP-B 3k-4l-t2-SMP-A & 3k-4l-t2-SMP-B 6k-2l-t2-SMP-A & 6k-2l-t2-SMP-B
Fibre volume fraction	1k-2l-t2-SMP-A & 1k-4l-t2-SMP-A & 3k-3l-t2-SMP-A & 3k-4l-t2-SMP-A 1k-4l-t2-SMP-B & 3k-2l-t2-SMP-B & 3k-4l-t2-SMP-B
Laminate thickness	1k-4l-t2-SMP-A & 1k-6l-t3-SMP-A
Fibre property & distribution	3k-4l-t2-SMP-A & 6k-2l-t2-SMP-A 3k-4l-t2-SMP-B & 6k-2l-t2-SMP-B

3. Experiments

3.1. Three-point bending tests

Bending was the dominant deformation form for the device, and therefore three-point bending tests were conducted. The specimens were cut following the ASTM D790 criterion into a dimension of 12.7 mm in width, 60 mm and 70 mm in length for thickness of 2 mm and 3 mm, respectively. Experiments were conducted on a Zwick/Rolle 010 universal testing machine with a 1kN load cell. The indenter and two support rollers of the three-point bending rig were all cylinder with a diameter of 10 mm. The span to depth ratio was 16:1 (32 mm and 48 mm for the laminate thickness of 2 mm and 3 mm, respectively). A temperature chamber with a range of −80 °C to 250 °C was used. Isothermal bending tests were conducted by first heating specimens to target temperatures (the same as the tensile tests for SMPs) at a heating rate of 3 °C/min. For a uniformly inner thermal distribution, samples were left at target temperatures for at least 20 min. Then they were preloaded at 2 N with a crosshead velocity of 2 mm/min followed by bending tests with the crosshead velocity of 1 mm/min. Trials were terminated when either the specimen broke, or the flexural strain reached 0.05 mm/mm.

3.2. Shape memory recovery tests

The shape memory characteristic is the key for self-deployment, and therefore it is necessary to assess the shape recovery speed and ratio at different temperatures. Firstly, it is essential to investigate the shape memory properties of pure SMPs at different temperatures because the shape memory effect comes from the polymer matrix. Besides, it is inferred that compared with pure SMPs, fibre reinforced laminates are more vulnerable to recovery. This is because more strain energy is stored in laminates due to fibre microbuckling, and carbon fibre is a good conductor of heat. Therefore, three kinds of samples (pure SMP-A, 1k-4l-t2-SMP-A and 1k-4l-t2-SMP-B) are selected for this analysis. By comparing 1k-4l-t2-SMP-A and 1k-4l-t2-SMP-B, the influence of the epoxy matrix can be investigated. The fibre effect can be obtained by contrasting pure SMP-A and 1k-4l-t2-SMP-A.

Tests were carried out with specimens in a rectangular shape of 15 mm in width and 60 mm in length. These specimens were then bent into a U shape with an inner diameter of 10 mm, which was the same as

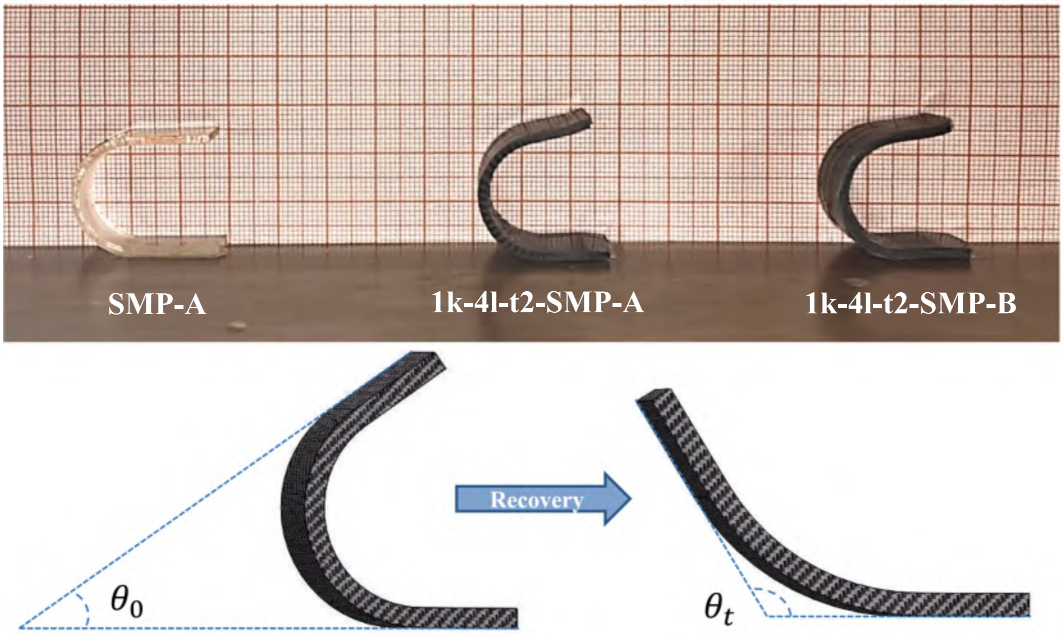

Fig. 7. Experimental and calculation methods for shape memory recovery.

SMPC release devices. The shaped temperatures were 120 °C and 80 °C for laminates based on SMP-A and SMP-B, respectively, following the analysis from material design. Shape memory recovery tests were carried out at 60 °C, 80 °C, 100°C and 120 °C. The reason why 20 °C and 40 °C were forsaken was because matrices were viscoelastic. According to the time–temperature equivalence principle, the shape recovery would take a very long time at such low temperatures. It was challenging to observe experimentally in a limited test duration. In addition, 140 °C and 160 °C were abandoned because these high temperatures would accelerate the ageing of resin matrices, which was not conducive to repeated usage. The experiments and calculation were conducted in Fig. 7, where a heating oven activated the recovery. The recovery ratio was calculated as follows by using recovery angles as in literature [20]:

$$R_r(t) = \frac{\theta_t - \theta_0}{180^\circ - \theta_0} \times 100\% \tag{14}$$

where θ_0 and θ_t denoted angles at the beginning and time t, respectively, whereas 180° represented the initial angle of the specimen in a flat shape.

3.3. *Preliminary verification on a symmetrical prototype*

The shape memory recovery stimulated by a heating oven cannot be used in engineering applications because of its heavy, bulky structure and integral heating, which will damage electronic components on spacecrafts. Therefore, resistor heaters are used to motivate the recovery of SMPC release devices under a 5 V DC power supply. These heaters were made of constantan insulated by polyimide film. The heaters had a thickness of about $150\mu m$, and was supplied by the Beijing Hongyu Aerospace Technology Co., Ltd. The power density was designed to be 0.92 W/cm^2 and the resistance was 7.7 Ω. An ultra-soft binding element called VHB produced by 3 M company was used to apply the heaters to SMPC surfaces. In this way, although the deformation of the heater was not coordinated with the SMPC, the super-elastic double-sided adhesive acted as a transition layer to avoid cracking of the contact interface. Besides, the structure was dominated by bending deformation, and the thin heaters had limited bending stiffness. Therefore, the stiffness of heaters had little effect on the shape recovery process.

Besides, resistor heaters were attached to both the upper and bottom surfaces of each SMPC release device to enhance the robustness of the heating system. The recovery carried out under atmosphere was labelled as SMPC-A-IO. In addition, the air pressure and temperature in aerospace were different from those in the atmosphere. These two environmental factors were important to the electrical heating and further the recovery of SMPC devices. The low temperature would weaken the heating performance of resistor heaters and postpone recovery. Therefore, recovery tests were also conducted in a thermal vacuum test system with an ultimate vacuum level of 10^{-6} Pa. The refrigeration was achieved by liquid nitrogen and mechanical methods. The temperature could be controlled from −150 °C to 150 °C with an accuracy of ±1 °C, stability of ±1 °C/h, and a heating or cooling rate of 3 °C/min. The degree of vacuum was less than $1 \times 10^{-3} Pa$ and the temperature was −92 °C.

Three specimens investigated recovery robustness in vacuum recovery tests. One was stimulated by two resistor heaters on both surfaces, labelled as SMPC-V-IO. The other two were activated by only one heater attached to the inner or outer surface, labelled as SMPC-V-I and SMPC-V-O, respectively. Moreover, to verify that SMPC release devices could deploy the structure successfully, two SMPC release devices attached with resistor heaters on each surface were assembled on a prototype. The deployments were recorded upon heaters powered.

4. Results and discussion

4.1. *Three-point bending characteristics*

The flexural stress σ_f, strain ε_f and modulus E_f of laminates can be calculated as:

$$\sigma_f = \frac{3FL}{2bh^2} \tag{15}$$

$$\varepsilon_f = \frac{6\delta h}{L^2} \tag{16}$$

$$E_f = \frac{mL^3}{4bd^3} \tag{17}$$

In these equations, F is the flexural load, L represents the support span, b and h denote the width and thickness of the specimen, respectively. δ is the predetermined centre deflection of the sample and is also

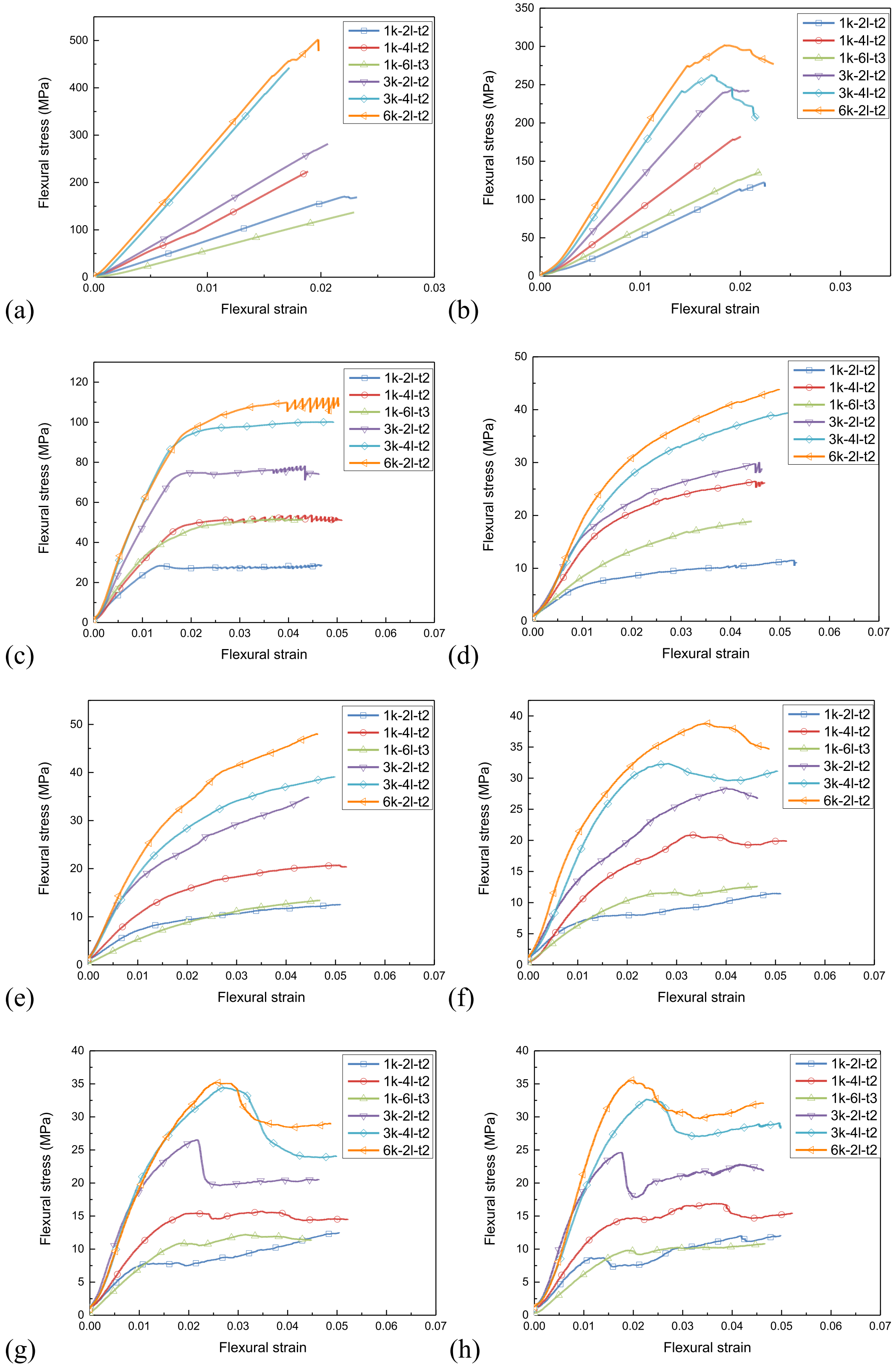

Fig. 8. Flexural stress versus flexural strain curves for fibre reinforced SMP-A at (a) 25 °C, (b) 40 °C, (c) 60 °C, (d) 80 °C, (e) 100 °C, (f) 120 °C, (g) 140 °C and (h) 160 °C.

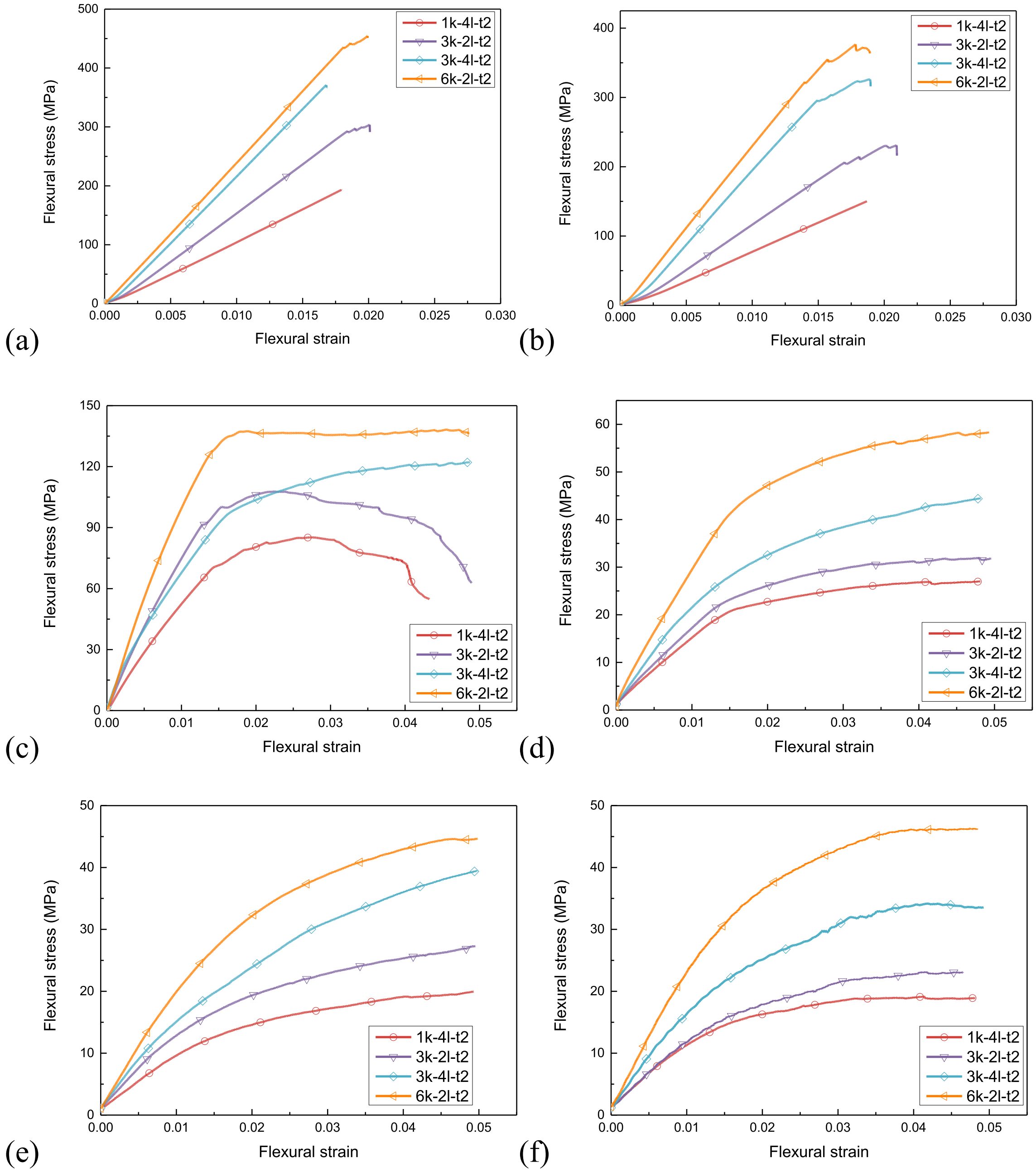

Fig. 9. Flexural stress versus flexural strain curves for fibre reinforced SMP-B at (a) 25 °C, (b) 40 °C, (c) 60 °C, (d) 80 °C, (e) 100 °C and (f) 120 °C.

the displacement of the indenter. m is the slope of the initial linear segment of the load–deflection curve.

The damage of laminates undergoing bending generally initiates from the compression surface, where fibres split, fray, kink or micro-buckle. At low temperatures, the matrices are in glassy state, and the stress can be transferred effectively. The deformation is dominated by carbon fibres in compression or tension. The laminates present a stiffening response at 25 °C (Fig. 8 (a) and Fig. 9(a)). At this temperature, specimens show cracks penetrating across the thickness at the indenter position in Fig. 10, indicating that the failure mode is brittle failure. When the temperature rises to 40 °C, samples exhibit strengthened response (Fig. 8 (b) and Fig. 9(b)), while only laminates with low fibre volume fraction show cracks penetrating through the thickness (Fig. 10). The failure mode of them is still brittle failure. In comparison, for laminates 3k-4l-t2 and 6k-2l-t2, the flexural stress versus strain curves exhibit plateaus after the linear period, which means that the failure mode transforms into the ductile failure. Besides, for these laminates (3k-4l-t2 and 6k-2l-t2), cracks only appear on the external surface (Fig. 10). Specimens yield with the increase of temperature. Laminates based on SMP-A and SMP-B experimented at 60 °C demonstrate different flexural stress–strain responses (Fig. 8 (c) and Fig. 9(c)). Specifically, fibre reinforced SMP-As in Fig. 8 (c) present jagged response curves, while laminates based on SMP-B (Fig. 9(c)) demonstrate smooth curves. These differences could be illustrated by the transformation of the failure mode. Kinking is known as a damage mode triggered by the local fibre breakage or buckling, or matrix shear. The critical stresses of kinking on the top compression surface σ_c^k and tension on the bottom surface σ_t^c along the fibre direction are calculated as [28]:

$$\sigma_c^k = \frac{\tau_{m,fail}}{\theta_i + \gamma} \tag{18}$$

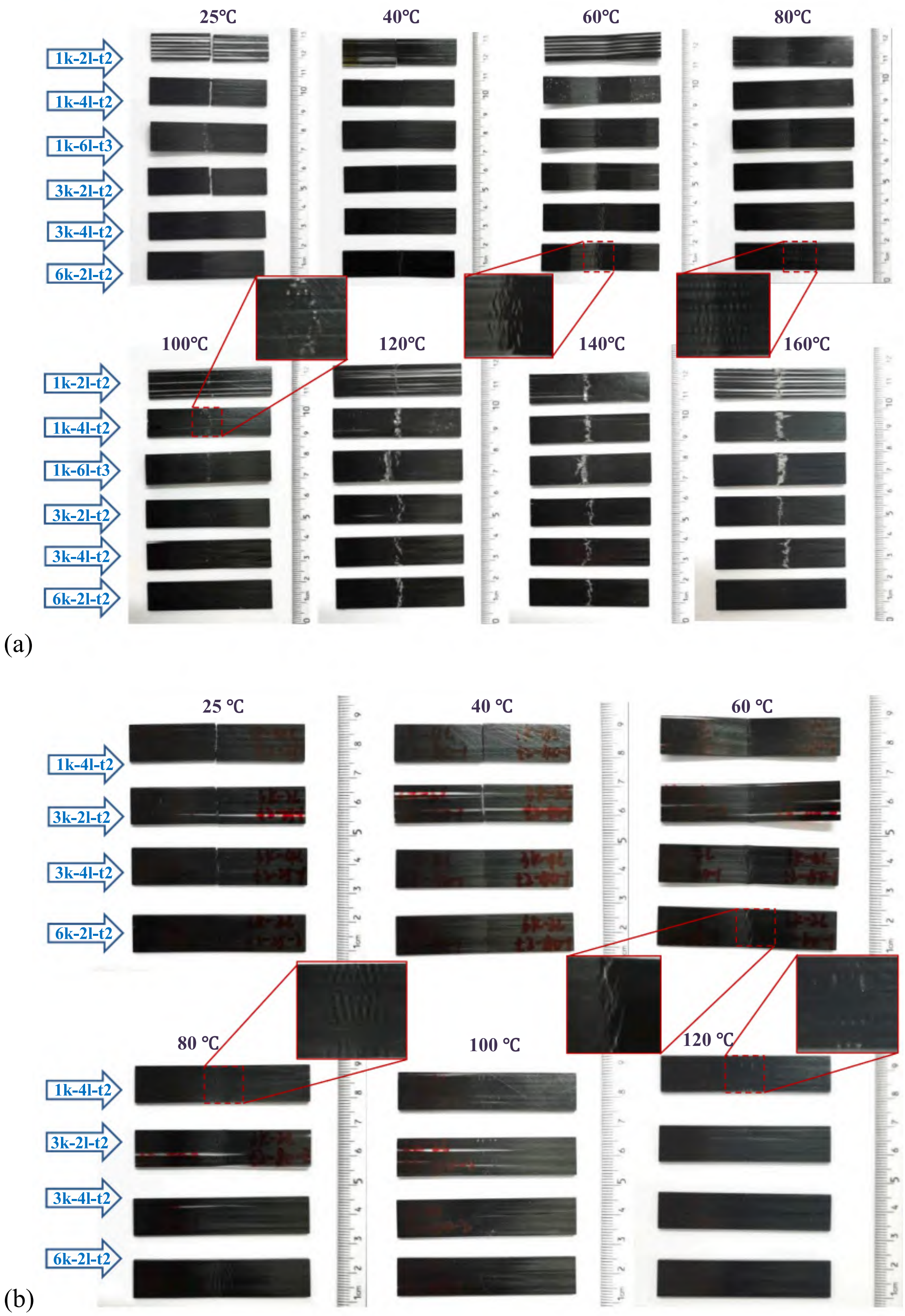

Fig. 10. Morphology of specimens undergone three-point bending, (a) laminates based on SMP-A and (b) laminates based on SMP-B.

$$\sigma_t^c = \sigma_t^f[v_f + (1\text{-}v_f)\frac{E_m}{E_f}] \qquad (19)$$

where $\tau_{m,fail}$ is the shear failure stress of matrix; θ_i denotes the fibre misalignment angle; γ represents the shear failure strain. σ_t^f means tensile strength of carbon fibres. The tensile strength of composites is insensitive to the matrix because the modulus of the matrix is much smaller than that of fibres. Therefore, the critical compression stress is

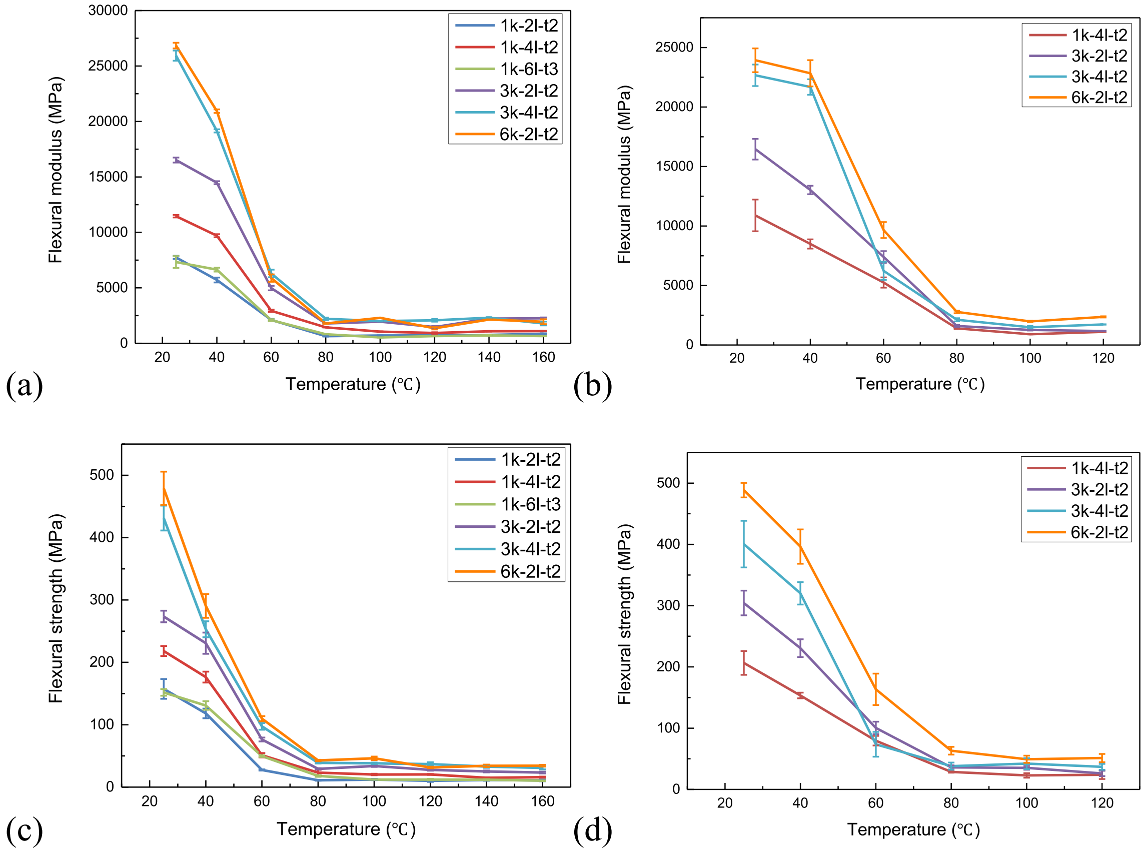

Fig. 11. Flexural modulus versus temperature curves for fibre reinforced (a) SMP-A, (b) SMP-B and flexural strength versus temperature curves for laminates based on (c) SMP-A and (d) SMP-B.

potentially larger than the tensile stress. The position of the failure depends on which of the two critical stresses is greater during the loading, and alternates between the top and bottom surfaces. The jagged stress–strain curves in Fig. 8 (c) are caused by this layer-by-layer failure.

As the temperature rises, the epoxy matrices enter their glass transition regimes and when laminates undergo bending deformation, large shear deformations mainly take place in the matrix. In the meanwhile, the soft matrix in the rubbery state cannot provide sufficient support to the stiff and slender carbon fibres. As a result, the fibres buckle, significantly reducing the flexural modulus of laminates. This is the key to laminates to withstand non-destructive deformations greater than the maximum strain of carbon fibres. At 80 °C (Fig. 8(d) and Fig. 9(d)) and 100 °C (Fig. 8 (e) and Fig. 9(e)), the specimens yield before reaching the maximum deflection and show uniform fibre microbuckled configuration. When it exceeds 120 °C (Fig. 8 (f-h) and Fig. 9(f)), the difference between laminates made up of two matrices appeares again. The load response of laminates based on SMP-A fluctuates, and the morphology also shows the extrusion failure of the matrix on the inner surface. While for SMP-B based laminates, there are smooth load curves, and their morphologies show negligible changes.

The flexural modulus and strength of laminates are shown in Fig. 11. Every curve presents a downward trend with a turning point around 80 °C, at which temperature, the matrix gradually undergoes the glass transition and becomes soft. For laminates with the same fibre distribution and tested at the same temperature, for instance, 1k-4l-t2-SMP-A and 1k-4l-t2-SMP-B at 25 °C, the modulus (Fig. 11(a) and (b)) and strength (Fig. 11(c) and (d)) show an insignificant difference. This similarity is reasonable because, according to the classical lamination theory (CLT), the matrix has limited contribution to the mechanical properties of laminates. After all, the modulus of carbon fibres is two orders of magnitude greater than that of matrices. Therefore, the relatively small difference between the two matrices has little influence on the flexural response of laminates. In addition, at the same temperature, the flexural modulus and strength increase with the growth of fibre volume fraction. The rate of increase, however, declines with the temperature. For example, for laminates based on SMP-A (Fig. 11(a)), compared with 1k-2l-t2, the modulus increases by 48.02% (1k-4l-t2), 5.41% (1k-6l-t3), 113.43% (3k-2l-t2), 234.97% (3k-4l-t2), and 246.69% (6k-2l-t2) at 25 °C. While at 120 °C, these rates of increase are 30.43% (1k-4l-t2), 9.11% (1k-6l-t3), 85.75% (3k-2l-t2), 139.46% (3k-4l-t2) and 89.34% (6k-2l-t2). This decline of the increase rate is natural and expected because, at high temperatures, the matrix softens. Thus, the bonding between fibres and matrix weakens, resulting in a declined enhancing effect. Besides, the increase of 1k-6l-t3 laminates is smaller because rotating plates cannot be thinner due to the manufacturing technique. When more layers are required, the laminates fabricated are thicker, resulting in a lower fibre volume fraction than the designed one. Additionally, the support span is different from the other laminates to ensure the same span-thickness ratio, introducing other experimental errors. Furthermore, laminates denoted as 3k-4l-t2 and 6k-2l-t2 possess the same fibre volume fraction and thickness; their mechanical response, however, varies. In general, 6k-2l-t2 laminates show a better reinforcing effect because the fibre T400HB-6K has a relatively higher tensile modulus and strength (Table. 1). Flexural stress versus strain curves in Fig. 9 reveal that the gap between 3k-4l-t2 and 6k-2l-t2 increases as the temperature rises. This difference can be illustrated by fibre microbuckling behaviour. The fibres are distributed more evenly in 3k-4l-t2 laminates. Thus, the microbuckled fibres enable the neutral surface to rush to the tensile surface when subjected to bending, reducing the stiffness significantly. Morphology indicates that uniform fibre microbuckling is more common in SMP-B based laminates (Fig. 10 (b)), so these specimens are selected for further analysis.

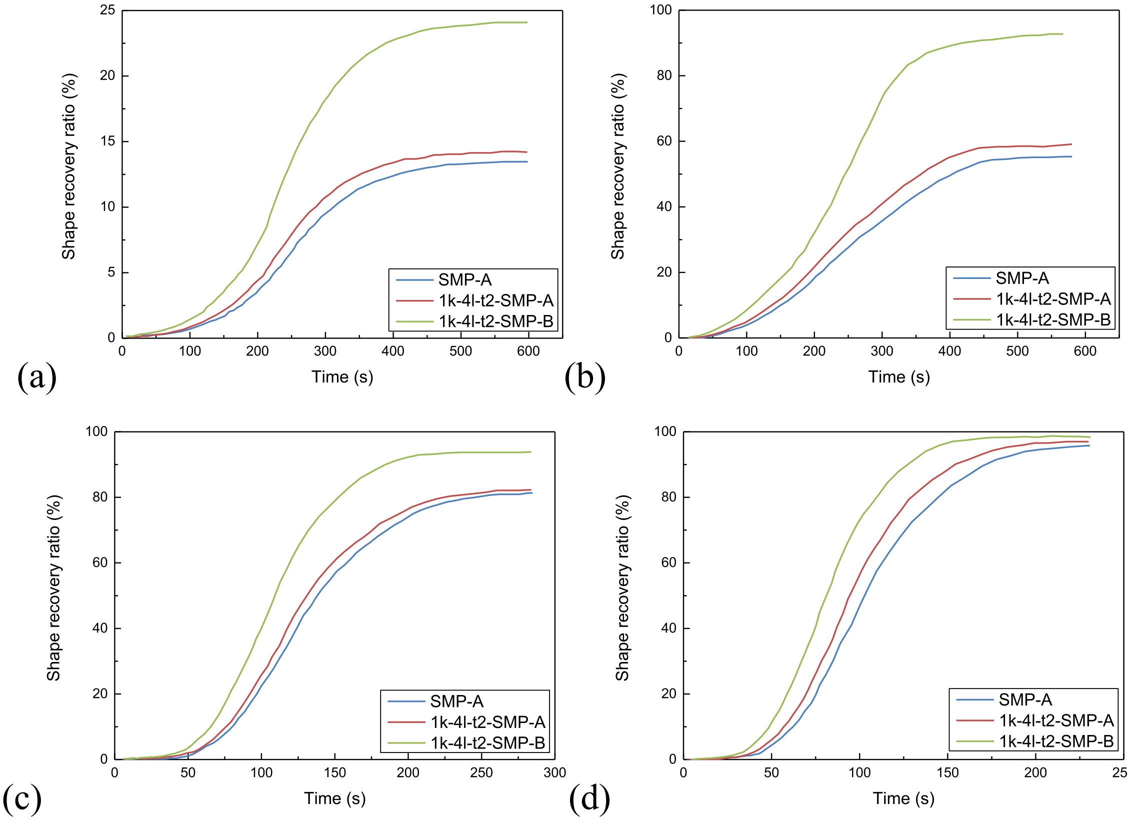

Fig. 12. Recovery ratio versus time curves of SMP-A, 1k-4l-t2-SMP-A and 1k-4l-t2-SMP-B at (a) 60 °C, (b) 80 °C, (c) 100 °C and (d) 120 °C.

4.2. Shape memory performance

Shape memory properties of SMP-A, 1k-4l-t2-SMP-A and 1k-4l-t2-SMP-B evaluated by recovery response are shown in Fig. 12. At all four temperatures studied, three kinds of laminates first undergo a slow reaction period, followed by a rapid recovery, and finally gradually stabilize to a certain value. With the increase of temperature, the recovery ratio of each specimen is amplified. All specimens can achieve a recovery ratio of greater than 98 % near the *Tg*. While at 60 °C, the stable recovery ratio is less than 12 % and 25 % for laminates based on SMP-A and SMP-B, respectively. It is worth noticing that for laminates based on SMP-A, the recovery ratio at 100 °C is significantly higher than at lower temperatures. The recovery ratio still increases at higher temperatures, but only to a limited extent. This turning temperature for laminates based on SMP-B is 80 °C. Besides, laminates based on SMP-A exhibit a slower response and lower stable recovery ratio. This is because SMP-A has a higher *Tg* than SMP-B, so they need a higher temperature to arouse the shape memory effect. In addition, for pure polymer and laminates both based on SMP-A (i.e., SMP-A and 1k-4l-t2-SMP-A), laminates always respond earlier than polymers. Two factors can cause this phenomenon. Firstly, the excellent thermal conductivity of carbon fibres enables composites to achieve internal thermal balance more quickly. Secondly, the strain energy stored due to the fibre microbuckling also speeds up the recovery. Furthermore, it can be reasonably inferred that shape memory response will be accelerated with the ncrease of fibre volume fraction.

4.3. Functional validation of deployable symmetrical structures

Synthesizing the above analysis, although SMP-A has a higher modulus than SMP-B, this contributes little to fibre reinforced composites. Instead, laminates based on SMP-A are more prone to fail under the same bending deformation. As for shape memory recovery, laminates based on SMP-A require higher activation temperature and longer reaction time. However, they can maintain the moulded configuration at relatively high temperatures. Therefore, laminates based on SMP-A are recommended for mechanisms requiring large load-bearing capacity and high working temperatures. While for mechanisms entailing large deploy/fold ratio and quick shape recovery response, laminates based on SMP-B with relatively lower fibre volume fraction are desired. The deployable structure in this work is for small satellites and subsystems, requiring low latching force. Therefore, a faster deployable demonstration is preferred. As a result, laminates 1k-4l-t2 based on SMP-B are prepared for functional validation.

Shape memory recovery of a single SMPC release device and assembled deployable prototype has been shown in Fig. 13. Release devices are activated by resistor heaters powered by 5 V DC voltage. The free recovery of the SMPC-A-IO in the atmosphere (Fig. 13 (a)) begins at 1 min, then continues a rapid deformation until 1 min 15 s and stops at 2 min. In contrast, the recovery in the vacuum chamber shows some differences. As shown in Fig. 13 (b), the recovery with two heaters (SMPC-V-IO) begins after heating for 1 min and is completed at 1 min 53 s. At the same time, those activated by only one heater are slower. SMPC device with the heater stuck on the inner surface (SMPC-V-I) responses also from 1 min and unfolds at about 2 min 13 s. The device with the heater on the outer surface (SMPC-V-O) shows a visible deformation at 2 min 13 s and finishes the extension at 3 min14s. It is found that the heater on the outer shell has stalling activation effect than that on the inner surface. This contrast is caused by the low temperature, and the outer surface contacts the chamber directly, resulting in more heat loss.

The power is switched off when the above times are reached, and the bending angles of each cooled sample after recovery are measured. The recovery ratio in Table. 3 is obtained using the same method as in Fig. 7 and Eq. (14). The devices activated by two heaters (SMPC-V-IO) show an about 90% recovery ratio, with a decrease of 3.22% for that in the atmosphere (SMPC-A-IO). SMPC-V-I presents an 83.05% recovery ratio

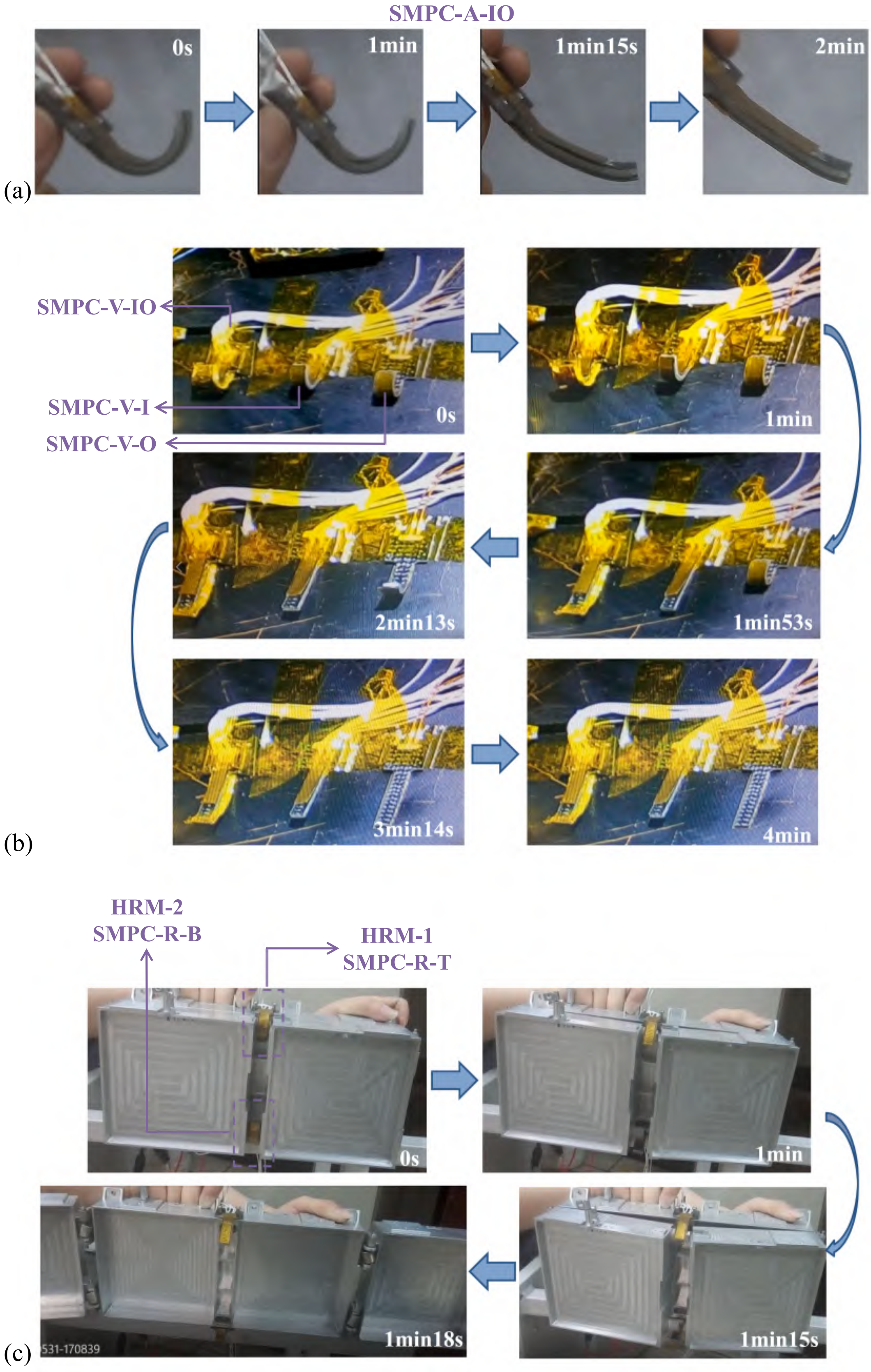

Fig. 13. SMPC release devices (a) recover in the atmosphere, (b) recover in a vacuum chamber at −92 °C and (c) trigger the deployment of a symmetrical prototype.

Table 3
Releasing properties of SMPC devices and the deployable structure.

Sample	SMPC-A-IO	SMPC-V-IO	SMPC-V-I	SMPC-V-O	SMPC-R-T	SMPC-R-B
Release time	2 min	1 min 53 s	2 min 13 s	3 min 14 s	1 min 18 s 233.31 ms	1 min 18 s 299.97 ms
Shape recovery ratio	92.86%	89.64%	83.05%	89.52%	74.21%	71.09%

after 2 min 13 s, while the SMPC-V-O demonstrate a ratio of 89.52% which is approaching the results of SMPC-V-IO. Additionally, the heaters on the inner surfaces retract when SMPCs recover the flat shape in Fig. 13. (b), indicating that adhesion by this double-sided tape on the inner surface reduces the shape recovery ratio. Overall, no matter which resistor heater is absent or invalid, whether in atmosphere or vacuum, the recovery can always be completed within 5 min with the ratio greater than 80%, demonstrating a robust recovery.

Further, a relatively rapid deployment is seen in the symmetrical structure in Fig. 13 (c). SMPC release devices also start to recover at 1 min. The difference from the free recovery is that at this time, the modulus of laminates drops sharply, and the deployment is accelerated under the effect of torsion spring hinges. A clear gap appears between the fixed module and deployable modules at 1 min 15 s. The gap widens rapidly after that, and the deployment is completed at 1 min 18 s. The release times for SMPC-R-T and SMPC-R-B are defined when the left and right deployable modules separate from the HRMs, respectively. The results in Table. 3 are obtained through the recorded video with a frame per second of 30 (accuracy of 33.33 ms), demonstrating a difference of 66.66 ms. Generally, this difference is not observable to the naked eyes. The recovery ratios for these two devices are also presented, with an about 20% decline compared with that of SMPC-A-IO. This is because the release is accelerated by the spring hinge, and the same results are found in the literature [20]. This preliminary demonstration proves that the design concept is valid for the inherently synchronous deployment. This mechanism is promising in aerospace applications with further engineering verification.

5. Conclusions

Design, fabrication, and preliminary engineering validation of SMPC release devices for synchronous deployed structures have been proposed with satisfactory results. This design concept is suitable for symmetrical mechanisms with two deployable modules. First, unidirectional carbon fibre reinforced composites are designed according to the fibre micro-buckling prediction. Therein, fibre volume fraction, laminate thickness and modulus ratio of fibres and matrices are the main factors affecting the mechanical properties of composites. Laminates made up of two epoxy resins with different *Tg*s from a similar system have been tested by three-point bending tests. The results show that laminates with higher *Tg* matrix possess relatively higher bending stiffness. In comparison, those based on lower *Tg* matrix can withstand more considerable bending deformation without failure. Besides, shape memory recovery tests reveal that laminates based on lower *Tg* matrix demonstrate rapid actuations and higher recovery ratios. Moreover, the addition of carbon fibres can also improve the recovery speed and ratio. Therefore, mechanical requirements, environmental temperatures, and deploy/fold ratio need to be considered for engineering applications. Laminates 1k-4l-t2 based on SMP-B are selected for preliminary functional validation in a symmetrical prototype. SMPC devices stimulated by attached resistor heaters in the atmosphere and vacuum show the robust recovery. Finally, the deployment on a symmetrical prototype is successfully demonstrated. This concept can be modified to synchronize the deployment of various structures to facilitate the subsequent attitude control.

Data availability

The raw/processed data required to reproduce these findings cannot be shared at this time as the data also forms part of an ongoing study.

CRediT authorship contribution statement

Dou Zhang: Conceptualization, Validation, Investigation, Writing – original draft. **Liwu Liu:** Conceptualization, Resources. **Xin Lan:** Conceptualization, Resources. **Jinsong Leng:** Supervision, Funding acquisition. **Yanju Liu:** Supervision, Funding acquisition.

Declaration of Competing Interest

The authors declare that they have no known competing financial interests or personal relationships that could have appeared to influence the work reported in this paper.

Acknowledgements

This work is supported by the Heilongjiang Touyan Innovation Team Program, the National Natural Science Foundation of China (Grant No. 11632005) and China Scholarship Council.

References

[1] Li YY, Wang C, Huang WH. Dynamics analysis of planar rigid-flexible coupling deployable solar array system with multiple revolute clearance joints. Mech Syst Sig Process 2019;117:188–209.
[2] Sun ZH, Zhang YQ, Yang DW. Structural design, analysis, and experimental verification of an H-style deployable mechanism for large space-borne mesh antennas. Acta Astronaut 2021;178:481–98.
[3] Sushko O, Medzmariashvili E, Filipenko L, Tsiklauri A, Medzmariashvili G, Nikoladze M, et al. Modified design of the deployable mesh reflector antenna for mini satellites. Ceas Space J 2021;13(4):533–42.
[4] Akizuki Y, Nagano H, Kinjo T, Sawada K, Ogawa H, Takashima T, et al. Development and testing of the re-deployable radiator for deep space explorer. Appl Therm Eng 2020;165.
[5] Ambrose J. Flex Heat Pipe East-West Deployable Radiator. Microgravity Sci Technol 2019;31(3):311–6.
[6] Bovesecchi G, Corasaniti S, Costanza G, Tata ME. A Novel Self-Deployable Solar Sail System Activated by Shape Memory Alloys. Aerospace 2019;6:78.
[7] Olson M. Flexible solar-array mechanism. In: Proceedings of the 7th aerospace mechanisms symposium; 1972. p. 233–49.
[8] Chmielewski A. Overview of Gossamer Structures. Prog Astronautics Aeronautics 2001.
[9] Liu T, Zhou T, Yao Y, Zhang F, Liu L, Liu Y, et al. Stimulus methods of multi-functional shape memory polymer nanocomposites: A review. Compos A Appl Sci Manuf 2017;100:20–30.
[10] Jani JM, Leary M, Subic A, Gibson MA. A review of shape memory alloy research, applications and opportunities. Mater Design 2014;56:1078–113.
[11] Gall K, Mikulas M, Munshi NA, Beavers F, Tupper M. Carbon fiber reinforced shape memory polymer composites. J Intell Mater Syst Struct 2000;11(11):877–86.
[12] Forintos N, Czigany T. Multifunctional application of carbon fiber reinforced polymer composites: Electrical properties of the reinforcing carbon fibers–A short review. Compos B Eng 2019;162:331–43.
[13] Leng J, Lan X, Liu Y, Du S. Shape-memory polymers and their composites: stimulus methods and applications. Prog Mater Sci 2011;56(7):1077–135.
[14] Lee J, Han J-H, Lee Y, Lee H. Separation characteristics study of ridge-cut explosive bolts. Aerosp Sci Technol 2014;39:153–68.
[15] Ogden S, Klintberg L, Thornell G, Hjort K, Bodén R. Review on miniaturized paraffin phase change actuators, valves, and pumps. Microfluidics Nanofluidics 2014;17(1):53–71.
[16] Stewart AC, Hair JH. Intricacies of using Kevlar cord and thermal knives in a deployable release system: issues and solutions. In: Proceedings of the 36th aerospace mechanism symposium; 2002. p. 15–7.
[17] Yoo YI, Jeong JW, Lim JH, Kim K-W, Hwang D-S, Lee JJ. Development of a non-explosive release actuator using shape memory alloy wire. Rev Sci Instrum 2013; 84:015005.
[18] Zhao H, Lan X, Liu L, Liu Y, Leng J. Design and analysis of shockless smart releasing device based on shape memory polymer composites. Compos Struct 2019;223: 110958.

[19] Wei H, Liu L, Zhang Z, Du H, Liu Y, Leng J. Design and analysis of smart release devices based on shape memory polymer composites. Compos Struct 2015;133:642–51.

[20] Zhang D, Liu L, Leng J, Liu Y. Ultra-light release device integrated with screen-printed heaters for CubeSat's deployable solar arrays. Compos Struct 2020;232:111561.

[21] Banik J, Murphey T. Synchronous deployed solar sail subsystem design concept. 48th AIAA/ASME/ASCE/AHS/ASC structures. In: Structural dynamics, and materials conference; 2007. p. 1837.

[22] Murphy DM, Murphey TW, Gierow PA. Scalable solar-sail subsystem design concept. J Spacecraft Rockets 2003;40(4):539–47.

[23] Lan X, Liu LW, Liu YJ, Leng JS, Du SY. Post microbuckling mechanics of fibre-reinforced shape-memory polymers undergoing flexure deformation. Mech Mater 2014;72:46–60.

[24] Chen JG, Liu LW, Liu YJ, Leng JS. Thermoviscoelastic shape memory behavior for epoxy-shape memory polymer. Smart Mater Struct 2014;23:055025.

[25] TORAYCA® yarn Product data.

[26] Li FF, Scarpa F, Lan X, Liu LW, Liu YJ, Leng JS. Bending shape recovery of unidirectional carbon fiber reinforced epoxy-based shape memory polymer composites. Compos A Appl Sci Manuf 2019;116:169–79.

[27] Jędral A, Bona A. Validation of Microscopy Measured Porosity in Carbon Fibbers Composites. J KONES 2019;26:83–90.

[28] Jia Z, Li T, Chiang FP, Wang L. An experimental investigation of the temperature effect on the mechanics of carbon fiber reinforced polymer composites. Compos Sci Technol 2018;154:53–63.